AGU100 ADVANCING EARTH AND SPACE SCIENCE

Geophysical Research Letters

RESEARCH LETTER
10.1029/2018GL081612

Key Points:
- Boreal summer ISO northward propagations are significantly deteriorated with decreased elevation of the TP
- Lowering the TP reduces the mean state vertical wind shear, the positive vorticity, and boundary layer moisture convergence, weakening northward propagation of the ISO
- Compared with the boundary layer moisture advection and air-sea interaction mechanism, the mean state vertical wind shear is most critical for the ISO northward propagation

Supporting Information:
- Supporting Information S1

Correspondence to:
B. Wang,
wangbin@hawaii.edu

Citation:
Yang, Y.-M., Wang, B., & Lee, J.-Y. (2019). Mechanisms of northward propagation of boreal summer intraseasonal oscillation revealed by climate model experiments. *Geophysical Research Letters*, *46*, 3417–3425. https://doi.org/10.1029/2018GL081612

Received 12 DEC 2018
Accepted 15 FEB 2019
Accepted article online 21 FEB 2019
Published online 22 MAR 2019

©2019. American Geophysical Union. All Rights Reserved.

Mechanisms of Northward Propagation of Boreal Summer Intraseasonal Oscillation Revealed by Climate Model Experiments

Young-Min Yang[1,2], Bin Wang[1,2], and June-Yi Lee[3,4]

[1]Key Laboratory of Meteorological Disaster of Ministry of Education and Earth System Modeling Center, Nanjing University of Information Science and Technology, Nanjing, China, [2]Department of Atmospheric Sciences and International Pacific Research Center, University of Hawai'i at Mānoa, Honolulu, HI, USA, [3]Research Center for Climate Sciences and Department of Climate System, Pusan National University, Busan, South Korea, [4]Center for Climate Physics, Institute for Basic Science (IBS), Busan, South Korea

Abstract Northward propagation of the boreal summer intraseasonal oscillation (ISO) has profound impacts on Northern Hemisphere extreme weather events. This study aims to test the hypotheses proposed in the previous studies to explain northward propagation of the ISO by drastically changing the climatological mean states through lowering the Tibetan Plateau (TP) with a fully coupled Earth system model, Nanjing University of Information Science and Technology Earth System Model version 3.0. The model reproduces realistic ISO over South Asia and the northern Indian Ocean. The results show that ISO northward propagations significantly weaken with decreased elevation of the TP. Lowering the TP reduces the vertical shear of the mean monsoon circulation over the northern Indian Ocean. The reduced vertical shear deteriorates the generation of positive vorticity anomalies and boundary layer moisture convergence to the north of ISO precipitation center, thereby weakening northward propagation of the ISO. On the other hand, the boundary layer moisture advection and air-sea interaction do not change appreciably when the TP elevation is reduced. These results suggest that the mean state vertical shear is most critical for the ISO northward propagation.

Plain language summary In boreal summer, a heavy precipitation belt slowly moves from the equatorial Indian Ocean to south Asian monsoon regions on a 2- to 6-week time scale, which affects extreme weather events over Asia. Therefore, understanding the causes of the northward movement of tropical precipitation belt is societally important. For this purpose, we performed a set of climate model experiments in which we reduced the topography over the Tibetan Plateau (TP). We found that northward movement of tropical precipitation significantly weakened with decreasing elevation of the TP. Lowering the TP changes the mean circulation over the eastern Indian Ocean. The changed mean circulation weakens boundary layer moisture convergence to the north of the precipitation belt, which deteriorates the northward movement of the tropical precipitation. We highlight that the mean state vertical shear is important for the northward movement of tropical precipitation anomalies.

1. Introduction

The eastern equatorial Indian Ocean (IO) is the most active center of boreal summer intraseasonal oscillation (BSISO; e.g., Wang & Rui, 1990; Zhu & Wang, 1993), which is represented by distinct northward propagation and affects the active and break phases of Indian summer monsoon (Ding & Wang, 2009; Kemball-Cook & Weare, 2001; Krishnamurti & Subramanian, 1982; Krishnan et al., 2000; Sikka & Gadgil, 1980; Wang et al., 2006; Yasunari, 1980, and many others). Beyond South Asia, the BSISO and its northward propagation can also affect the beginning of the East Asian summer monsoon (Wang et al., 2017; Li et al., 2015; Wang & Xie, 1997) and northward movement of the subtropical monsoon rain belt (e.g., Yang et al., 2010) and significantly modulate tropical cyclone activities over the Indian, Pacific, and Atlantic Oceans (Goswami et al., 2003; Kikuchi et al., 2009; Maloney & Hartmann, 2001; Moon et al., 2018) as well as the extratropical circulation (Moon et al., 2013).

The dynamic theory based on modification of intraseasonal oscillation (ISO) by summer mean states attributes northward propagation primarily to the impact of the vertical shear of monsoonal flows on ISO (Drbohlav & Wang, 2005; Jiang et al., 2004; Wang & Xie, 1997). Wang and Xie (1997) explained that the

northward propagation is a result of Rossby wave emanation from an Madden Julian Oscillation (MJO)-like convective system and the Kelvin-Rossby wave couplet, particularly from Sumatra and the dateline where the equatorial convection weakens. Lawrence and Webster (2002) showed that about 80% of northward propagation events are linked to the MJO events moving eastward, which supports the hypothesis proposed by Wang and Xie (1997). Why does the emanated Rossby-wave convective anomaly propagate northward? In the presence of an easterly vertical shear, a heating-induced baroclinic Rossby wave can generate barotropic vorticity through coupling the baroclinic and barotropic mode (Wang & Xie, 1996; Xie & Wang, 1996). Using reanalysis data, Jiang et al. (2004) found that a barotropic vorticity anomaly indeed occurs to the north of ISO precipitation center, inducing boundary layer (BL) moisture convergence, and promotes convective development, driving ISO convection northward. Using an idealized model, Drbohlav and Wang (2005) further revealed that the vertical advection of mean easterly vertical shear by ISO vertical motion can induce barotropic divergence to the north of convection, confirming this "monsoon vertical shear" mechanism for the BSISO northward propagation. Kang et al. (2010) and Liu et al. (2015) suggested that a secondary meridional circulation by convective momentum transports results in low-level convergence under the presence of easterly shear. DeMott et al. (2013) analyzed results from a coupled climate model simulation and found that BL moisture advection and the barotropic vorticity effect contribute to northward propagation dominantly. Liu et al. (2017) and Abhik et al. (2013) proposed that the BSISO propagates northward by shallow convection, which occurs at the north of the BSISO convective center.

Air-sea interaction has been also suggested to explain the northward propagation of ISO. Kemball-Cook et al. (2002) suggested that sea surface temperature (SST) may increase at the north of the ISO convection center by increased solar radiation and reduced surface heat fluxes with decreasing wind speed, which results in BL moisture convergence (BLMC) and favors for convection moving northward. The studies that compared atmosphere only with coupled GCM showed that warm SST anomalies by air-sea interaction destabilize the lower troposphere to the north of convection, which leads to northward propagation (Fu et al., 2003; Fu & Wang, 2004; Zheng et al., 2004).

The Nanjing University of Information Science and Technology Earth System Model (NESM3.0) has recently been developed for multidisciplinary numerical simulations (Cao et al., 2018). The NESM3.0 simulates not only reasonable climatology but also realistic MJO and BSISO (Yang & Wang, 2018). Signals of the northward propagation in boreal summer are strong and well organized over the IO.

The goal of this study is to perform coupled climate model experiments to test the hypotheses concerning the northward propagation of the BSISO, which invoke the roles of the vertical wind shear, meridional moisture advection, and air-sea interaction. The strategy is to drastically change the climatological mean states through lowering the Tibetan Plateau (TP) orography. The reduced orography can change not only a model's climatology, particularly wind fields, but also its ISO simulation. The two questions are mainly discussed in this study. How do changes of mean state affect ISO northward propagation? And which processes are dominant for northward propagation among the various mechanisms reviewed in this research?

The climate model NESM3.0 was introduced, and the data and model experiment were described in section 2. We explain how the change of mean state affects the ISO northward simulation based on dynamics-based diagnostics in section 3. We discuss the mechanisms responsible for changing northward propagation in section 4, and we summarize our findings.

2. The Model and Diagnostic Methods

2.1. Model and Experiments

The NESM3.0 consists of atmosphere, ocean, land, and sea ice component, and they are fully coupled with each other. The details of the model are described in Cao et al. (2018), Yang and Wang (2018), and Yang et al. (2018). The atmosphere model has T63 horizontally and 47 levels vertically. The horizontal and vertical resolutions of ocean model are 1° and 46 layers, respectively. Note that meridional resolution of ocean model is about 1/3° over the equatorial region. The sea ice model has about 1° horizontally and four sea ice layers vertically.

Three experiments were carried out by using the NESM3.0 with different orography data to examine the impacts of mean state on ISO northward propagation: (1) the NESM3.0 with observed orography (TP100),

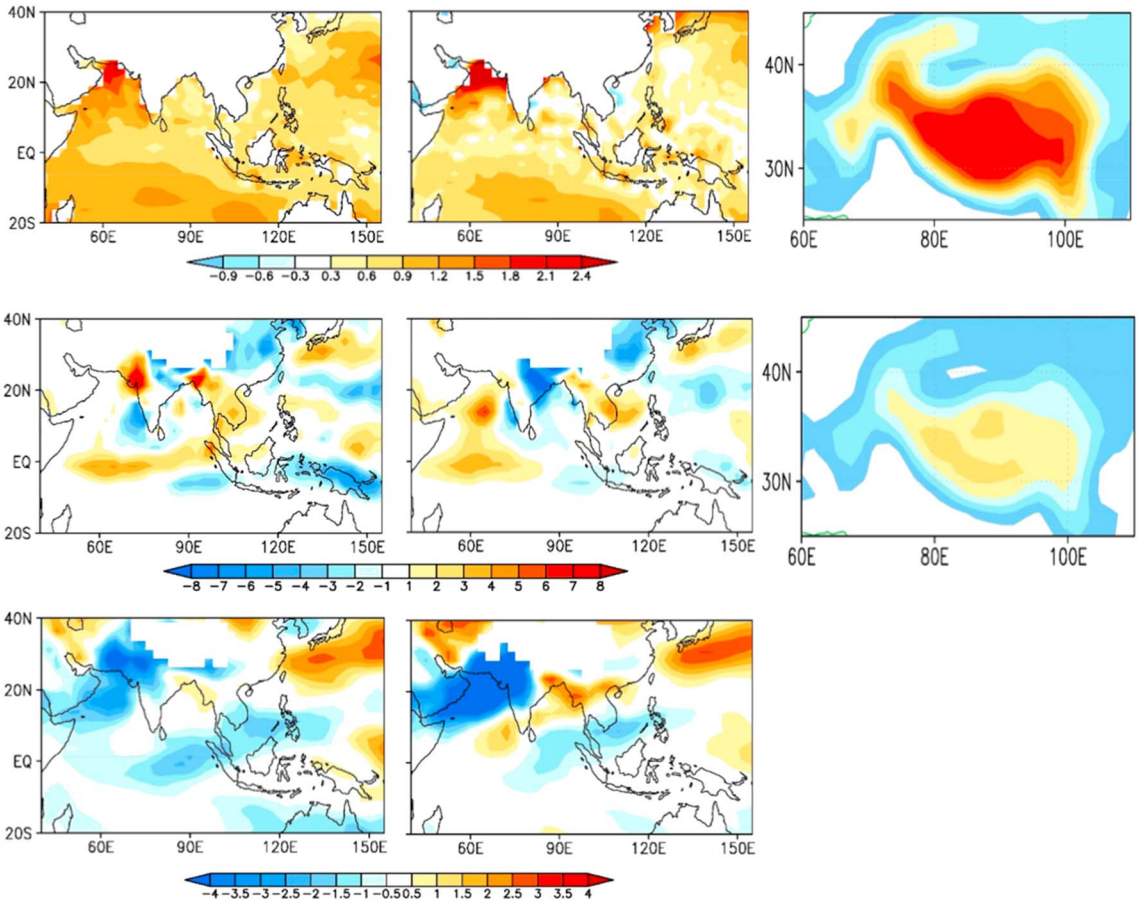

Figure 1. Difference in July–August mean state sea surface temperature (K, upper panels) precipitation (mm/day, middle panels), and zonal wind at 850 hPa (m/s, lower panels) between (a) TP50–TP100 and (b) TP00–TP100. (c) Horizontal map of orography (m) over Tibet Plateau region used in the original (observed, upper panels) and reduced (50%) value (middle panels).

(2) orography reduced by 50% (TP50), and (3) flat orography (TP00) over TP region (60–110°E, 25–45°N). Note that the orography at the boundaries is smoothed based on Cannon et al. (2017) to inhibit numerical noises (Figure 1c). Also note that all external data (e.g., orographic standard deviation, slope, anisotropy, angle, peaks elevation and valleys elevation, and mean orography data) used for gravity wave drag effect are reduced accordingly. The model configuration and parameter values are the same for each experiment. In all experiments 50-year integrations have been conducted with the fixed external forcings (1990s). We used the last 20-year simulation data for analysis. A historical run using the CMIP6 protocols was utilized for the initial condition.

2.2. The Data and Diagnostic Methods

We used the Global Precipitation Climatology Project daily data (Adler et al., 2003) for precipitation. We also utilized the European Center for Medium-Range Weather Forecast Reanalysis Interim data (Dee et al., 2011) for calculating circulation anomalies (1997–2014). To obtain the ISO signal during the summer season (1 May to 31 October), we applied a 20- to 70-day band-pass filter. We adapted dynamics-based diagnostics to evaluate the model's results as well as analysis for climatological mean state of precipitation, SST, and surface winds.

3. Changes of the Climatology and ISO by Lowering TP Orography

The July–August mean state differences in SST, precipitation, and zonal wind between TP100 and TP50 (or TP00) are presented in Figure 1. In the TP50 experiment, the reduced topography causes relatively strong

warming over the Arabian Sea, western and south IO, and East Asia Sea. There is a weak warming from the equatorial eastern IO to Bay of Bengal, but the meridional gradient of SST is insignificant (Figure 1a). Precipitation increases in western India and the Indo-China peninsula and decreases over the Maritime Continent and eastern China and Korea. There is a strong anomalous easterly wind over the Arabian Sea, eastern IO, and Maritime continent indicating that the lowered TP topography weakens monsoon westerly flows. Over East Asia, the anomalous southward and eastward winds, which indicate the weakening of the western Pacific subtropical high, reduce rainfall over East China and Korea. In the TP50, the positive precipitation anomalies in the western Pacific and negative precipitation anomalies in the Maritime Continent induce anomalous easterly wind over the equatorial IO, which can suppress eastward propagation of ISO. In the TP00, the warming in SST over the Arabian Sea is stronger than TP50 and associated easterly anomalies are strengthened. Precipitation increases in the western Pacific and Indo-China peninsula. Note that there is no significant meridional gradient of SST warming in the eastern IO (Figure 1b).

4. Changes in BSISO Properties

To obtain insight into the evolution and propagation of the BSISO in the models, composite life cycles of outgoing longwave radiation (OLR) and winds at 850 hPa (U850) are used (Figure 2). We defined eight phases based on the BSISO index calculated by multivariate empirical orthogonal function analysis of daily anomalies of OLR and U850 (10°S to 10°N, 40°E to 160°E) for May–October (Lee et al., 2013). In the observation, ISO convective anomalies occur in the equatorial western IO at phase 1 and move eastward and intensify, reaching peak intensity at phases 2 and 3 in the Eastern Indian Ocean (EIO). The strong convection anomaly moves northward from the EIO to the Bay of Bengal and extends eastward to the northern Maritime continent at phase 3. The extended convective anomalies to the south of the Philippine Sea then shift northward to subtropical western Pacific from phases 4 and 6 and eventually weaken and disappear at phases 7 and 8. The differences in the life cycles of BSISO among model simulations are mainly found in the northward propagation. The TP100 realistically reproduces the observed counterpart. The ISO occurs in the western equatorial IO. The convection anomalies move northward to the northern IO from the EIO. In the TP50, the northward propagation in the EIO and eastward propagation from EIO to Philippine Seas are both weaker than those in TP100. The TP00 simulation shows a "standing" ISO and fails to simulate eastward propagation and northward propagation. The TP00 may fail to simulate northward propagation of the ISO because of its weak initial intensity rather than incorrect processes associated with northward propagation of the ISO (e.g., incorrect vorticity by reduced weak zonal shear). To identify this issue, we made additional composite life cycles of the OLR and lower-level circulation (TP00_S; Figure S1 in the supporting information), which include only strong initial ISO events from TP00 simulation data. In TP00_S, the initial intensity at phases 1–3 is stronger than TP00 but the convective anomalies do not move northward over East IO. At phases 2 and 3, observation shows positive vorticity anomalies in the eastern IO (or Bay of Bengal) but both TP00 and TP00_S fail to simulate positive anomalies there. These results suggest that the standing feature of the ISO in the TP00 is mainly attributed to incorrect vorticity anomalies rather than weak initial intensity of ISO. The details will be discussed in section 4.

Figure 3 shows the observed meridional lead-lag correlation diagrams of ISO precipitation. The ISO precipitation center at the EIO (80°E to 100°E, 5°S to 5°N) was used as a reference because the organized northward propagation of the ISO starts from the EIO and the ISO is strong. It is observed that the ISO precipitation propagates northward with 1 m/s between 5°N and 20°N. In the TP100 (Figure 3b), the model simulates systematic northward propagation of the ISO precipitation in the EIO with a slightly weak magnitude and slower phase speed of about 0.8 m/s. However, the TP50 produces weaker northward propagation of ISO than TP100. In the TP00, propagation of precipitation is very weak; the ISO convection in the EIO does not move northward. The results indicate that the reduced orography deteriorates the ISO simulation significantly.

5. Causes of the Changes of ISO Simulations With Reduced Orography

We examined circulation and thermodynamic fields to understand how the ISO simulations changed. The reduced orography over the TP region changes the circulation significantly, particularly mean vertical zonal wind shear for the boreal summer (March-October) (Figure 4a). The vertical shear is defined by the difference

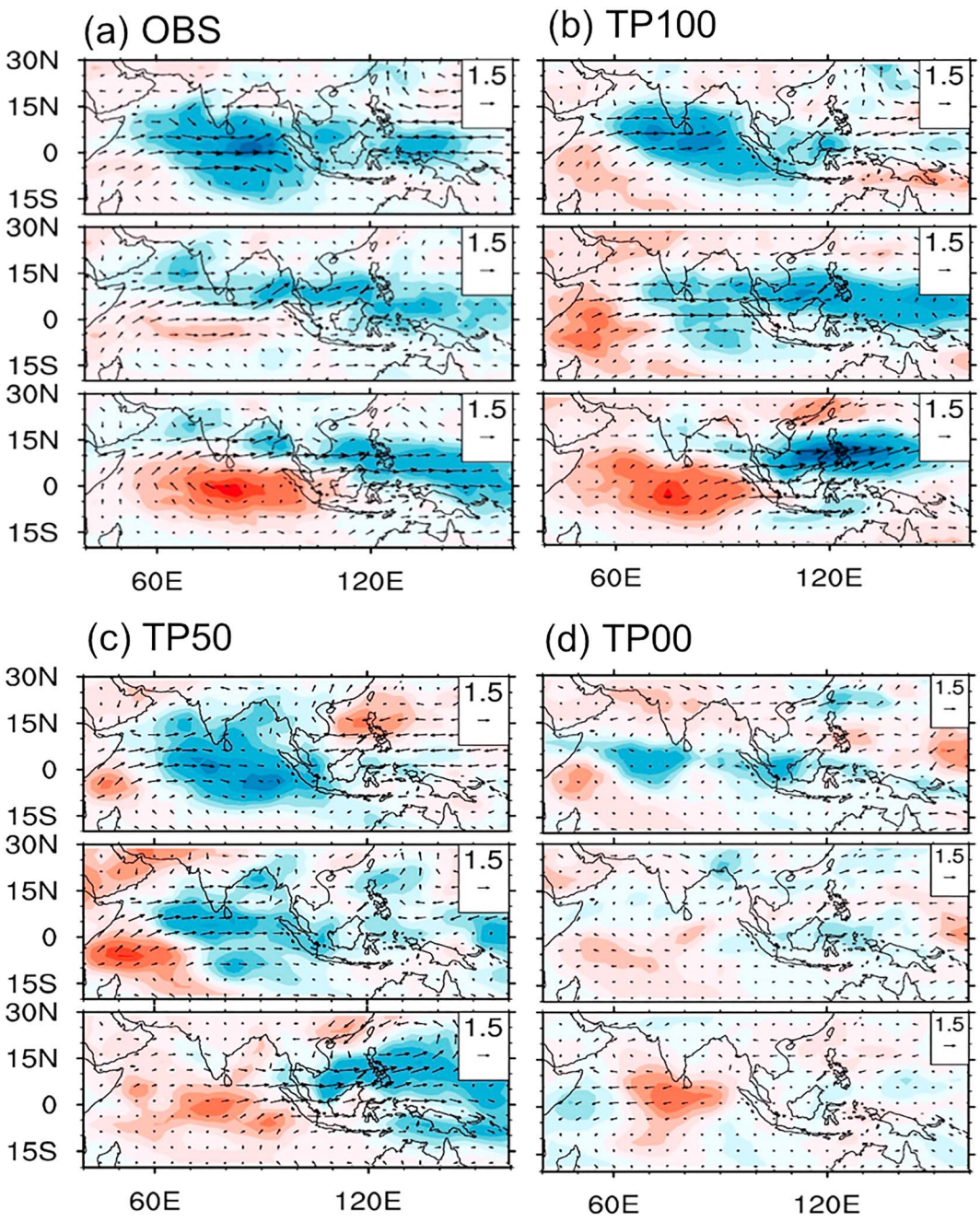

Figure 2. The life cycle composite of outgoing longwave radiation (shading) and 850-hPa wind (vector) anomaly. We defined eight phases of intraseasonal oscillation based on Lee et al. (2013). Upper (lower) panel represents phase 3 (5).

in zonal winds between 200 and 850 hPa (U_{200}–U_{850}) averaged over 80°E and 100°E. The easterly vertical shear occurs between 10°S and 20°N and has a peak near 5°N. The TP100 reproduces the observed vertical wind shear well except the maximum easterly vertical shear slightly shifts to the north (8°N). In the TP50 the magnitude of the easterly shear deceases by 40% and was reduced by 60% in the TP00. The reduced vertical wind shear is mainly attributed to the weakened easterly wind in the upper troposphere rather than westerly wind in the lower troposphere (figure not shown) due to the reduced TP dynamic and thermodynamic effects.

The presence of vertical zonal wind shear can induce the coupled baroclinic and barotropic modes, generating a barotropic vorticity anomaly (Wang & Xie, 1997; Xie & Wang, 1996). Figure 4b shows the vorticity at 850 hPa averaged over 80–100°E associated with the 20- to 70-day filtered precipitation averaged over the

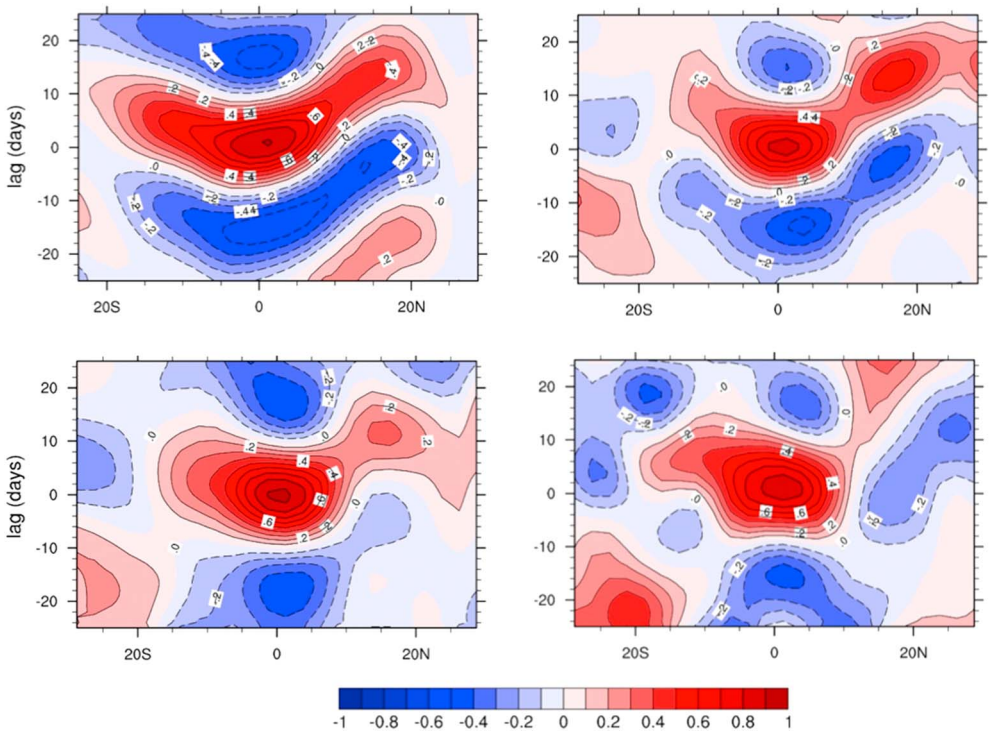

Figure 3. Propagation of intraseasonal oscillation precipitation as depicted by the lead-lag correlation of 20- to 70-day filtered precipitation averaged over 80–100°E from (a) observation and model simulations with (b) observed topography, (c) 50% of observed topography, and (d) no topography over the Tibet plateau region during boreal summer (May–October). The ISO precipitation averaged over 80°E to 100°E and 5°S to 5°N was used as a reference for calculating the correlation.

eastern IO (5°S to 5°N, 80°E to 100°E). Strong positive (cyclonic) vorticity anomalies are located at north of the ISO precipitation center and extend northward to 15°N as found by Jiang et al. (2004). The TP100 experiment reproduces the observed pattern of the vorticity reasonably well. The magnitude is quite similar to the observed, but the maximum slightly shifts northward by about 3° of latitude, consistent with the bias in the simulated vertical wind shear. The magnitude of vorticity in the TP50 is reduced by about 50% and almost vanishes in the TP00 experiment. The model experiments show that the cyclonic vorticity is reduced with decreasing vertical wind shear, implying that the vertical shear of the mean circulation is responsible for vorticity generation to the north of the ISO center.

The change in vorticity can affect the generation of BLMC at 925 hPa (Figure 4c). The observed BLMC shows a peak around the ISO center and a northward extension, indicating that the consecutive convection may be generated to the north of the current ISO center. The ISO simulated in the TP100 experiments reproduces the observed extension of BLMC well although the model overproduces the BLMC. In contrast, the TP50 produces a very weak northward extension of BLMC and TP00 does not simulate the BLMC to the north of the ISO convection center, consistent with its failure in simulating the barotropic cyclonic vorticity. Note that the peak in the BLMC is located at the south of the corresponding cyclonic vorticity in both observation and model simulations, implying that another mechanism may also partly contribute to the generation of the BLMC (e.g., moisture-convection feedback).

The upward transport of the heat and moisture from BL to lower troposphere can be induced by BLMC. The abundant moisture in the lower troposphere increases equivalent potential temperature (EPT), which induces an increase of convective instability to the north of the ISO center (Hsu & Li, 2012). Figure 4 shows the meridional distribution of the convective instability index (EPT at 850 hPa and EPT at 300 hPa), which represents destabilization in advance of the ISO deep convection. In observation, convective instability is negative at the ISO precipitation center but positive to its north (5–20°N), suggesting that deep convection could develop to the north of the existing ISO deep convection. The TP100 captures the observed pattern

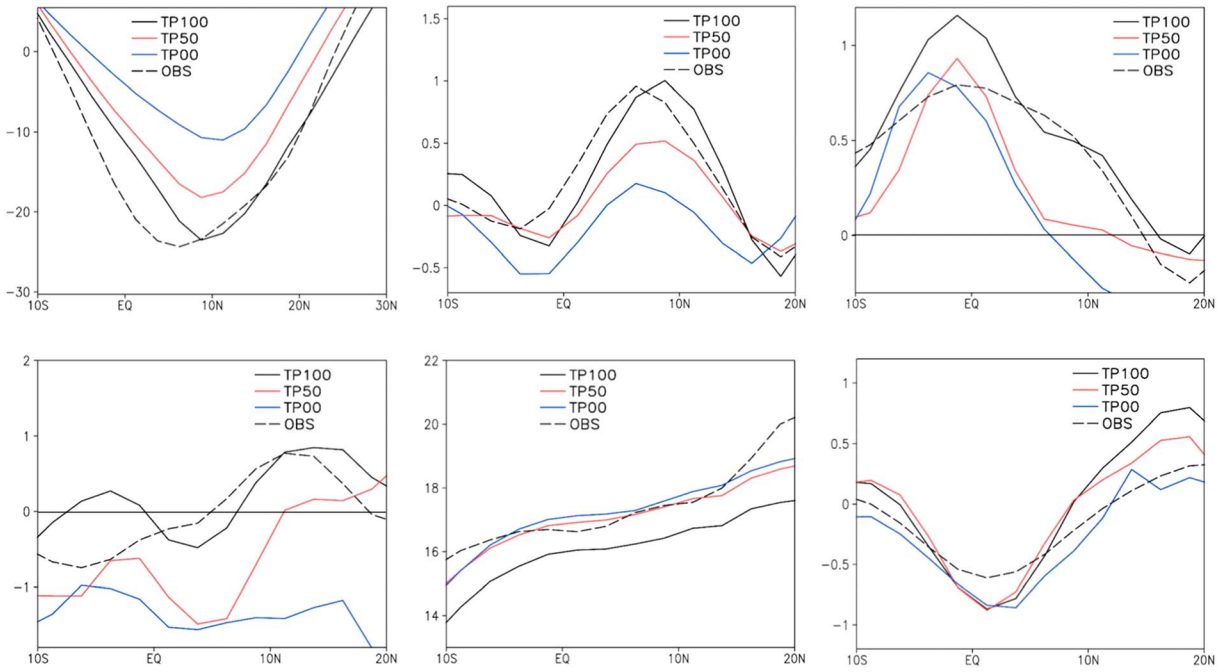

Figure 4. Meridional structure of May–November mean zonal shear (U_{200}–U_{850}; panel a) and mean specific humidity (panel e) averaged over 80–100°E from observation (dashed black line) and models. Meridional variation of the regressed ISO relative vorticity (s^{-1}) at 850 hPa (panel b), BL moisture convergence (day^{-1}) at 925 hPa (panel c), the convective instability index (panel d), and SST (panel f) averaged over 80–100°E from observation (dashed black) and model simulations. The 20- to 70-day filtered precipitation anomaly averaged over 5°S to 5°N and 80°E to 100°E was used as a reference for calculating regression. BLMC = boundary layer moisture convergence; SST = sea surface temperature.

of convective instability pretty well at the north of ISO center. However, the TP100 underproduces the convective instability over 2–10°N and overproduces it over 10–20°N, which is consistent with the meridional distribution of the BLMC. The TP50 produces negative convective instability except north of 10°N. The TP00 does not simulate the positive convective instability to the north of the ISO center, indicating that the ISO northward propagation may not be generated.

Other northward propagation mechanisms may be also involved. Here we briefly discuss whether other processes can contribute to changes of northward propagation in the EIO. We first examined BL moisture advection by the BSISO winds due to the meridional gradients of the mean specific humidity (DeMott et al., 2013; Jiang et al., 2004). The meridionally asymmetric specific humidity may generate BLMC to the north of the ISO convection center, which induces northward propagation. The meridional pattern of May–October mean specific humidity averaged over 80–100°E was shown in Figure 4e. The meridional gradients of the specific humidity are similar to each other. The mean specific humidity profiles in TP50 and TP00 are larger than TP100 over the latitude range from 10°S to 20°N and closer to the observation, suggesting that the meridional structure of BL moisture from all experiments is favorable with subsequent ISO northward propagation. Therefore, the BL moisture advection mechanism may not explain the weakened northward propagation in TP50 and TP00 and may not be a major process in governing ISO northward propagation.

Regarding the air-sea interaction mechanism, we examine the meridional structure of the SST regressed on the equatorial ISO convection averaged over 80°–100°E (Figure 4f). In observations, cold SST anomalies occur at the ISO precipitation center but warm SST anomalies to its north (20°N), implying that the deep convection may be stimulated to propagate northward. Note that the negative SST at the center is mainly due to heavy clouds that reduce the downward shortwave radiation heating. The enhanced evaporation cooling can also reduce the SST. The TP100 reproduces the observed SST reasonably well but overproduces the anomalies over 10–20°N. The TP50 and TP20 simulate similar meridional structure of SST with TP100. The magnitudes in TP50 and TP00 are smaller over 10–20°N than that in TP100 but are still comparable with observation. This result implies that warm SST anomalies in the TP50 and TP00 over 10–20°N are favorable

to northward propagation. However, this is inconsistent with the result of weakened or failed northward propagation shown in Figures 3 and 4, indicating that the interaction between atmosphere and ocean may be a minor mechanism in supporting ISO northward propagation in this experiment.

6. Conclusion and Discussion

In this study, the role of vertical zonal wind shear on northward propagation of ISO in the Eastern IO is investigated through analysis of the NESM3.0 numerical simulations. The NESMv3.0 model simulates realistic northward propagation of the ISO precipitation over EIO with a slightly slower speed of about 0.8 m/s^{-1} from EIO to the Bay of Bengal. The reduced TP topography weakens the vertical wind shear over the EIO, and the corresponding northward propagation of the ISO precipitation is weakened or becomes standing in the EIO.

Analysis of the northward propagating ISO structure from the model experiments demonstrates that the meridionally asymmetric vorticity induced by the mean vertical wind shear is critical for northward propagation of ISO convection. The strong mean easterly vertical shear in the monsoon region during boreal summer generates cyclonic vorticity by coupling the barotropic and baroclinic modes. The cyclonic vorticity induces enhanced BLMC that enhances the lower tropospheric EPT or moist static energy. The increase in lower tropospheric EPT generates positive convective instability to the north of the ISO precipitation, which leads to ISO northward propagation. The results suggest that the vertical shear of zonal winds is a key factor for the ISO northward propagation.

This study also tested other proposed mechanisms that attempt to explain the northward propagation of ISO. We examined the mechanism of meridional moisture advection of the mean specific humidity by ISO winds. The TP50 and TP00 experiments showed similar meridional structure of mean specific humidity as in TP100, but the corresponding northward propagations are substantially weakened. This suggests that the mean meridional specific humidity is not a dominant factor for ISO northward propagation. Similarly, for the air-sea interaction processes, all three simulations simulate positive SST anomalies to the north of the ISO precipitation center, which is not consistent with their corresponding simulated northward propagations shown in Figure 3. This implies that the air-sea interaction processes are not essential for simulating northward propagation in this model.

The numerical experiments were made with a single model. Future research could conduct similar studies using different climate models to examine the degree of model-dependence of the results. Generally speaking, the ISO simulation is sensitive to convective parameterizations (including the shallow convective scheme) as well as other physical processes and warrants further studies. We noted that there are significant changes in northward propagation over the western Pacific (WP, 130–150°E) in the reduced TP orography experiments (not shown). We found that the reduced orography deteriorates the ISO simulation significantly. We speculate that the mechanism for northward propagation over the WP may be different from that over the EIO (DeMott et al., 2013). More detailed investigations will be done in future studies.

Acknowledgments
This work is funded by the National Key Research and Development Program of China (grant 2016YFA0600401), the National Natural Science Foundation of China (grant 41420104002), and the National Science Foundation (Climate Dynamics Division) Award AGS-1540783. This is Earth System Modeling Center (ESMC) publication no. 252, SOEST publication no. 10667, IPRC publication no. 1369, and J. Y. Lee acknowledges the support from the Institute for Basic Science (project code IBS-R028-D1) and the National Research Foundation (2015R1C1A2A01053980) in Korea. The data are available at https://figshare.com/articles/day_tp100_nc/7658345.

References

Abhik, S., Halder, M., Mukhopadhyay, P., Jiang, X., & Goswami, B. (2013). A possible new mechanism for northward propagation of boreal summer intraseasonal oscillations based on TRMM and MERRA reanalysis. *Climate Dynamics*, *40*(7-8), 1611–1624. https://doi.org/10.1007/s00382-012-1425-x

Adler, R. F., Huffman, G. J., Chang, A., Ferraro, R., Xie, P.-P., et al. (2003). The version-2 global precipitation climatology project (GPCP) monthly precipitation analysis (1979–present). *Journal of Hydrometeorology*, *4*(6), 1147–1167. https://doi.org/10.1175/1525-7541(2003)004<1147:TVGPCP>2.0.CO;2

Cannon, F., Carvalho, L. M. V., Jones, C., Norris, J., Bookhagen, B., & Kiladis, G. N. (2017). Effects of topographic smoothing on the simulation of winter precipitation in High Mountain Asia. *Journal of Geophysical Research: Atmosphere*, *122*, 1456–1474. https://doi.org/10.1002/2016jd026038,2017

Cao, J., Wang, B., Yang, Y.-M., Ma, L., Li, J., Sun, B., et al. (2018). The NUIST Earth System Model (NESM) version 3: Description and preliminary evaluation. *Geoscience Model Development*, *11*(7), 2975–2993. https://doi.org/10.5194/gmd-11-2975-2018

Dee, D. P., Uppala, S. M., Simmons, A. J., Berrisford, P., Poli, P., Kobayashi, S., et al. (2011). The ERA-Interim reanalysis: Configuration and performance of the data assimilation system. *Quarterly Journal of the Royal Meteorological Society*, *137*(656), 553–597. https://doi.org/10.1002/qj.828

DeMott, C. A., Stan, C., & Randall, D. A. (2013). Northward propagation mechanisms of the boreal summer intraseasonal oscillation in the ERA-Interim and SP-CCSM. *Journal of Climate*, *26*, 1973–1992.

Ding, Q., & Wang, B. (2009). Predicting extreme phases of the Indian *summer monsoon*. *Journal of Climate*, *22*, 346–363.

Drbohlav, H.-K. L., & Wang, B. (2005). Mechanism of the northward propagating intraseasonal oscillation: Insights from a zonally symmetric model. *Journal of Climate*, *18*, 952–972.
Fu, X., & Wang, B. (2004). Differences of boreal summer intraseasonal oscillations simulated in an atmosphere–ocean coupled model and an atmosphere-only model. *Journal of Climate*, *17*, 1263–1271.
Fu, X., Wang, B., Li, T., & McCreary, J. P. (2003). Coupling between northward-propagating, intraseasonal oscillations and sea surface temperature in the Indian Ocean. *Journal of the Atmospheric Sciences*, *60*, 1733–1753.
Goswami, B. N., Ajayamohan, R. S., Xavier, P. K., & Sengupta, D. (2003). Clustering of synoptic activity by Indian summer monsoon intraseasonal oscillations. *Geophysical Research Letters*, *30*(8), 1431. https://doi.org/10.1029/2002GL016734
Hsu, P.-C., & Li, T. (2012). Role of the boundary layer moisture asymmetry in causing the eastward propagation of the Madden-Julian oscillation. *Journal of Climate*, *25*(14), 4914–4931.
Jiang, X., Li, T., & Wang, B. (2004). Structures and mechanisms of the northward propagating boreal summer intraseasonal oscillation. *Journal of Climate*, *17*, 1022–1039.
Kang, I.-S., Kim, D., & Kug, J.-S. (2010). Mechanism for northward propagation of boreal summer intraseasonal oscillation: Convective momentum transport. *Geophysical Research Letters*, *37*, L24804. https://doi.org/10.1029/2010GL045072
Kemball-Cook, S. R., & Weare, B. C. (2001). The onset of convection in the Madden–Julian Oscillation. *Journal of Climate*, *14*(5), 780–793.
Kemball-Cook, S., Wang, B., & Fu, X. (2002). Simulation of the Intraseasonal Oscillation in the ECHAM-4 model: The impact of coupling with an ocean model. *Journal of Atmospheric Science*, *59*, 1433–1453.
Kikuchi, K., Wang, B., & Fudeyasu, H. (2009). Genesis of tropical cyclone Nargis revealed by multiple satellite observations. *Geophysical Research Letters*, *36*, L06811. https://doi.org/10.1029/2009GL037296
Krishnamurti, T. N., & Subramanian, D. (1982). The 30–50 day mode at 850 mb during MONEX. *Journal of the Atmospheric Sciences*, *39*(9), 2088–2095. https://doi.org/10.1175/1520-0469(1982)039<2088:TDMAMD>2.0.CO;2
Krishnan, R., Zhang, C., & Sugi, M. (2000). Dynamics of breaks in the Indian summer monsoon. *Journal of the Atmospheric Sciences*, *57*, 1354–1372.
Lawrence, D. M., & Webster, P. J. (2002). The boreal summer intraseasonal oscillation: Relationship between northward and eastward movement of convection. *Journal of the Atmospheric Sciences*, *59*, 1593–1606.
Lee, J. Y., Wang, B., Wheeler, M. C., Fu, X., Waliser, D. E., & Kang, I.-S. (2013). Real-time multivariate indices for the boreal summer intraseasonal oscillation over the Asian summer monsoon region. *Climate Dynamics*, *40*, 493–509.
Li, K., Li, Z., Yang, Y., Xiang, B., Liu, Y., & Yu, W. (2015). Strong modulations on the Bay of Bengal monsoon onset vortex by the first northward-propagating intra-seasonal oscillation. *Climate Dynamics*, *47*, 107–115.
Liu, F., Wang, B., & Kang, I.-S. (2015). Role of barotropic convective momentum transport in the intraseasonal oscillation. *Journal of Climate*. https://doi.org/10.1175/JCLI-D-14-00575.1
Liu, F., Zhao, J., Fu, X., & Huang, G. (2017). The role of shallow convection in promoting the northward propagation of boreal summer intraseasonal oscillation. *Theoretical Applied Climatology*. https://doi.org/10.1007/s00704-017-2064-2
Maloney, E. D., & Hartmann, D. L. (2001). The Madden–Julian Oscillation, barotropic dynamics, and North Pacific tropical cyclone formation. Part I: Observations. *Journal of the Atmospheric Sciences*, *58*, 2545–2558.
Moon, J.-Y., Wang, B., Ha, K.-J., & Lee, J.-Y. (2013). Teleconnections associated with Northern Hemisphere summer monsoon intraseasonal oscillation. *Climate Dynamics*, *40*, 2761–2774. https://doi.org/10.1007/s00382-012-1394-0
Moon, J. Y., Wang, B., Lee, S.-S., & Ha, K.-J. (2018). An intraseasonal genesis potential index for tropical cyclones during northern hemisphere summer. *Journal of Climate*, *31*(22), 9055–9071.
Sikka, D. R., & Gadgil, S. (1980). On the maximum cloud zone and ITCZ over Indian longitude during the southwest monsoon. *Monthly Weather Review*, *108*, 1840–1853.
Wang, B., & Rui, H. (1990). Dynamics of the coupled moist Kelvin–Rossby wave on an equatorial β-plane. *Journal of the Atmospheric Sciences*, *47*(4), 397–413. https://doi.org/10.1175/1520-0469(1990)047<0397:DOTCMK>2.0.CO;2
Wang, B., Webster, P., Kikuchi, K., Yasunari, T., & Qi, Y. (2006). Boreal summer quasi-monthly oscillation in the global tropics. *Climate Dynamics*, *27*(7-8), 661–675. https://doi.org/10.1007/s00382-006-0163-3
Wang, B., & Xie, X. (1996). Low-frequency equatorial waves in vertically sheared zonal flow. Part I: Stable waves. *Journal of the Atmospheric Sciences*, *53*, 449–467.
Wang, B., & Xie, X. (1997). A model for the boreal summer intraseasonal oscillation. *Journal of the Atmospheric Sciences*, *54*, 72–86.
Wang, H., Liu, F., Wang, B., & Li, T. (2017). Effect of Intraseasonal Oscillation on South China Sea Summer Monsoon Onset. *Climate Dynamics.*. https://doi.org/10.1007/s00382-017-4027-9
Xie, X., & Wang, B. (1996). Low-frequency equatorial waves in vertically sheared zonal flow. Part II: Unstable waves. *Journal of the Atmospheric Sciences*, *53*, 3589–3605.
Yang, J., Wang, B., Wang, B., & Bao, Q. (2010). Biweekly and 21-30-day variations of the subtropical summer monsoon rainfall over the Lower reach of the Yangtze River Basin. *Journal of Climate*, *23*, 1146–1159.
Yang, Y.-M., & Wang, B. (2018). Improving MJO simulation by enhancing the interaction between boundary layer convergence and lower tropospheric heating. *Climate Dynamics*. https://doi.org/10.1007/s00382-018-4407-9
Yang, Y-M., B. Wang, Li, J. (2018). Improving seasonal prediction of East Asian summer rainfall: Experiments with NESM3.0. *Atmosphere,* Accepted.
Yasunari, T. (1980). A quasi-stationary appearance of 30 to 40 day period in the cloudiness fluctuation during the summer monsoon over India. *Journal of the Meteorological Society of Japan*, *58*, 225–229.
Zheng, Y., Waliser, D. E., Stern, W., & Jones, C. (2004). The role of coupled sea surface temperatures in the simulation of the tropical intraseasonal oscillation. *Journal of Climate*, *17*, 4109–4134.
Zhu, B., & Wang, B. (1993). The 30-60-day convection seesaw between the tropical Indian and western Pacific Oceans. *Journal of the Atmospheric Sciences*, *50*, 184–199.